Journal of Applied Polymer Science

Structural aspects of mechanical properties of iPP-based composites. I. Composite iPP fibers with VGCF nanofiller

Elena Ivan'kova,[1,2] Igor Kasatkin,[3] Olga Moskalyuk,[1,4] Vladimir Yudin,[1,2] Jose Maria Kenny[1,5]

[1]Mechanics of Polymers and Composite Materials, Institute of Macromolecular Compounds RAS, St. Petersburg, 199004 Russia
[2]Institute of Physics, Nanotechnology and Telecommunications, Saint Petersburg State Polytechnical University, St. Petersburg, 195251 Russia
[3]Department of Crystallography, Saint Petersburg State University, St. Petersburg, 199034 Russia
[4]Institute of Information Technology and Automation, Saint Petersburg State University of Technology and Design, St. Petersburg, 191186 Russia
[5]Materials Science and Technology Center, University of Perugia and European Center for Nanostructured Polymers, Terni, 05100 Italy
Correspondence to: E. I. (E-mail: ivelen@mail.ru)

ABSTRACT: Nanocomposite fibers consisting of isotactic polypropylene (iPP) as a matrix filled with vapor grown carbon nanofibers (VGCF) have been prepared and their fine crystalline structure and mechanical properties characterized. The obtained results point out that the VGCF oriented along the fiber extrusion direction induce crystallization in the surrounding iPP matrix in a special way leading to the formation of oriented iPP α-transcrystallite layers. The VGCF content and the draw ratio (DR) affect the textural properties of the composite material and lead to the formation of an anisotropic structure. The improvements of the mechanical properties of the composite fibers in both undrawn and drawn states are attributed to the VGCF aligning effect during extrusion, which produces highly oriented iPP crystalline structure, rather than to the reinforcing effect of the nanofibers. A new detailed scheme explaining the changes in tensile strength from the structural point of view is proposed. © 2015 Wiley Periodicals, Inc. J. Appl. Polym. Sci. **2015**, *132*, 41865.

KEYWORDS: composites; crystallization; mechanical properties; morphology; structure-property relations

Received 21 August 2014; accepted 6 December 2014
DOI: 10.1002/app.41865

INTRODUCTION

Polymer composite materials have partially or completely replaced many other materials in various applications such as engineering, aeronautics and textile industry, electronics, and medicine. In the last decades, composites containing carbon nanoparticles with unique properties (carbon nanotubes (CNT), nanofibers (CNF), fullerenes, graphenes, and others) have attracted particular attention of researchers and technicians.

Most studies of nanocomposites containing anisotropic carbon nanoparticles (CNF or CNT) have focused on improving electrical and mechanical properties.[1–9] Numerous investigations have been done on isotactic polypropylene (iPP) as a common plastic and semicrystalline polymer matrix. The results have shown that nanotubes and nanofibers could improve the tensile modulus of iPP and in some cases the strength, but usually with a loss of deformation at break.[10–12] The polymer matrix and the reinforcement are considered as two separate elements which may interact with each other only in terms of load transfer. Another important factor affecting the mechanical behavior of the polymer composite materials loaded with nanoparticles is the microstructural features of the polymer matrix which can be changed by the nano-size fillers.[13,14]

Differential scanning calorimetry (DSC) and electron microscopy experiments have shown that carbon nanoparticles (CNT, CNF) can act as effective nucleating agents in PP matrix.[13,15–20] In an isothermal crystallization study Lozano and Barrera observed, that the addition of 5 wt % CNF led to higher nucleation rate of PP and increased crystallization temperature by 8°C.[13] Sui *et al.* found an 18°C increase in the PP crystallization temperature with an addition of 5 wt % CNF.[15] However, there was no significant effect of CNFs on the melting temperature and on the degree of crystallinity.[15,16] Sandler *et al.* reported a strong aligning of the polymer chains and of the nanofibers along the drawing direction in a highly oriented PP film containing 0.5 wt % CNF.[17] Then, the polymer crystallized to produce lamellae perpendicular to the main molecular axis direction. The quality of the crystalline lamellae in the close proximity to the nanofiber surface was changed. This was related to an increase in crystallinity, as the spacing between the lamellae was reduced near the nanofiber.[21] It was shown that transcrystallization in PP depended on the surface

structure of carbon fibers—only high-modulus carbon fibers induced such transcrystallinity.[22]

Thermogravimetric (TGA) measurements confirmed the formation of a complex structured interface between iPP and VGCF and revealed the complex structure of that interface.[23] A thin hard layer was identified and assigned to the polymer segments captured by the nanofibers at such small distances. The van der Waals interaction between these macromolecules and the nanofiber is comparable with the energy of covalent bonds in the molecules of the polymer. The presence of a soft layer extending from the nanofiber-polymer interface at distances comparable with the radius of gyration of PP was also reported.[24]

The crystalline structure of the composite PP fibers was intensively studied by a number of authors.[25,26] Simultaneous SAXS and WAXS measurements during iPP melt spinning showed that the degree of crystallite orientation was controlled by the nucleation process.[25] The amount of the oriented crystals increased with addition of VGCF.[26]

Up to now, most of the above results on the crystallization behavior were obtained at a constant content of CNF. Only few researches were focused on the influence of the nanofiller content. In addition, a comprehensive study of the mechanical and crystallization behavior of PP filled with carbon nanoparticles was rarely reported. However, the mechanical properties of semicrystalline PP depend strongly on its microstructure and crystallinity. Consequently, a better understanding of the changes in the crystalline morphology of the polymers filled with anisotropic nanoparticles and their effect on the mechanical behavior of the composite materials is of great importance.

Since the properties of the final polymeric fiber are strongly influenced by the production conditions, it is necessary to better understand the evolution of the fine structure to optimize the fiber processing. In this work we report the effect of different amounts of anisotropic nanoparticles (VGCF) on the microstructure and mechanical properties of iPP/VGCF fibers in both unoriented and oriented states.

VGCF are found to significantly influence the fine structure of the iPP matrix in the composite fibers that allows fine tuning of the mechanical characteristics. The reinforcement role of VGCF is revealed to be negligible owing to a low adhesion between the matrix and the nanofillers. A scheme describing in detail the tensile strength changes is suggested.

EXPERIMENTAL

Material

The isotactic polypropylene Balen 01270 ($M_w = 250{,}000$ g mol^{-1}; Ufa Petroleum Refinery, Bashneftekhim, Ufa, Russia) produced in the form of granules was used as the polymer matrix. The graphitized carbon nanofibers produced by gas phase synthesis (vapor grown carbon fibers) (Showa Denko K.K., Japan) were used as a filler.[27] VGCF nanofibers had a shape of a cylinder with 100–150 nm in diameter and the axial ratio of about 30.

Sample Preparation

Samples of pure iPP and composites with VGCF were fabricated by melt-processing using a twin-screw microcompounder (DSM Xplore, The Netherlands) and a receiving unit from the same company. The amount of filler was varied as 1, 3, 5, 10, 20 wt %. The polymer granules were mixed with VGCF powder in the microcompounder for 5 min at 200°C at a screw rotation rate of 75 rpm. After the initial fiber had been formed through a die of 1 mm in diameter, the material was subjected to an additional orientation drawing by rewinding between two rollers, passing through a tunnel furnace at 150°C. The orientation drawing of the material occurred in the heated zone owing to the preset difference in the roller rotation rates producing different draw ratios (DR) of the fibers. The processing conditions were chosen in order to product good fibers with round and constant section. All samples of the fibers based on pure iPP and filled with VGCF were obtained in the same conditions.

Mechanical Properties

Mechanical characteristics of the composite fibers were determined at room temperature under uniaxial extension with the universal mechanical testing machine 1958-U-10 (Russia). The fiber strength σ_{br} was averaged over the testing results of 10 specimens of each fiber. The initial base length of the samples was 35 mm, and the velocity of the fiber extension was 10 mm min^{-1}.

Scanning Electron Microscope (SEM)

Investigations of the sample structure were carried out with the scanning electron microscope SUPRA 55VP (Carl Zeiss, Germany). The samples were covered by a thin layer of metal (Au or Pt) in order to prevent charging.

For the study of the inner fiber structure, the samples were broken perpendicularly to the fiber axis or tired along it in liquid nitrogen to prevent a plastic deformation of the specimens.

To reveal the surface structure of the fibers in more detail, they were etched in a mixture of $KMnO_4$ and H_3PO_4 following the procedure described in Ref. 28.

The fibers were held in vertical position for the SEM investigations.

WAXS

The crystalline structure of the pure iPP and composite fibers was studied by X-ray diffraction using the following diffractometers: (1) RIGAKU R-AXIS RAPID II with Co-K_α radiation and a large-area cylindrical imaging plate detector for obtaining two-dimensional WAXS patterns; (2) BRUKER D8 DISCOVER with Cu-K_α source to obtain one-dimensional patterns (θ–2θ scans) and azimuthal diffraction profiles. The first was used for the study of the fibers texture, since a two-dimensional pattern contained the full textural information at once. The θ–2θ scans obtained with the other (high resolution) diffractometer were used for the profile fitting and crystallite size analysis, since the instrumental contributions to the peak shapes were much smaller when using that instrument, and they could be easily evaluated. The results obtained with the two different instruments agreed perfectly well. The fibers were held in vertical position.

The full width at half-maximum (FWHM) of the 110 peak was used for calculation of the apparent transverse D_{110} sizes of the iPP crystallites with the Scherrer equation.[29]

RESULTS AND DISCUSSION

Mechanical Properties

Figure 1 demonstrates the dependence of the fiber strength (σ_{br}) on the content of the filler (%VGCF). It is clearly seen

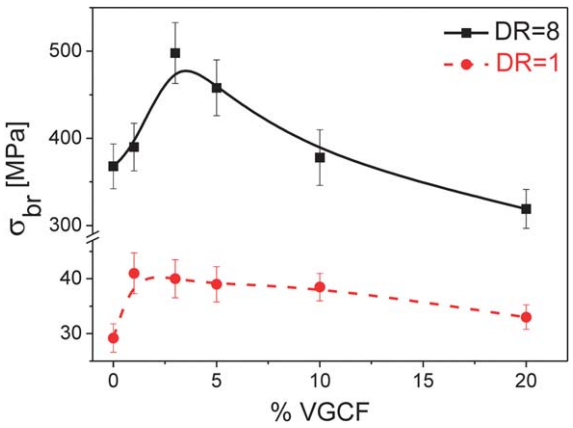

Figure 1. The dependence of the fiber strength (σ_{br}) on the content of the filler (%VGCF). [Color figure can be viewed in the online issue, which is available at wileyonlinelibrary.com.]

that the addition of only 1 wt % VGCF results in the considerable enhancement of the fiber strength σ_{br} in both undrawn (DR = 1) and drawn (DR = 8) states, but a maximum is reached at 3 wt % VGCF. Further increase in the filler content leads to the significant reduction of the mechanical strength. To clarify this situation, the fine structure of the studied polymeric and of the nanocomposite fibers was investigated in detail as it will be discussed later.

The drawn (DR = 8) composite fibers with the maximum σ_{br} = 500 MPa (3 wt % VGCF) were also mechanically tested at other draw ratios and compared with the drawn fibers of the pure iPP. It was found that the melt-spun pure iPP fibers could be drawn up to DR = 4 and DR = 8. However, the fibers containing 3 wt % VGCF could be drawn up to DR = 4, 8, and 12. Figure 2 demonstrates the influence of the draw ratio on the strength of the pure iPP and composite iPP + 3%VGCF fibers. It is seen that at low draw ratio DR = 4 the strength of the pure iPP and of the composite fibers differs weakly. However, at DR = 8 the strength of the composite fiber is 1.4 times higher than that of the pure iPP. This indicates that the drawing is more effective for the composite fiber compared with the pure one.

As mentioned above, the pure iPP fiber could not be drawn further in contrast to the composite iPP + 3%VGCF fiber that was stretchable up to DR = 12. However, the next drawing step did not produce a considerable effect on the strengthening of the composite fiber.

Scanning Electron Microscopy (SEM)

The effect of the nanofiller content on the mechanical properties of the investigated melt-spun fibers suggests a different structural evolution in the pure iPP and in the composites in both undrawn and drawn states.

Figure 3(a–c) shows the SEM micrographs of the surface structure of the undrawn pure iPP and of the two composite fibers containing 3 wt % VGCF and 20 wt % VGCF, respectively. One can clearly see the spherulite structure on the surface of the pure iPP and of the iPP matrix of the composite fibers. At the same time, the VGCF nanofibers well aligned along the extrusion direction of the fibers can be observed. The micrographs obtained from both composite fibers (3 wt % and 20 wt % VGCF) are rather similar. The main difference between them is in the amount of the revealed VGCF nanofibers.

Figure 4 presents the SEM micrographs of the cross-sections of the composite fibers showing a uniform distribution of individual VGCF in the iPP matrix. No VGCF agglomerates are observed. The preferred orientation of VGCF in the extrusion direction (normal to the cross-section plane) is seen. However, it is easily noted that the VGCF pulled out from the iPP matrix indicating the weak adhesion. This suggests that the strong preferred orientation of VGCF along the filament direction and the weak adhesion to the matrix will play concurrent roles in the strengthening process of the resulting composites.

Figure 5(a–d) shows the SEM micrographs of the internal structure of the composite fibers (3 wt % and 20 wt % VGCF) revealed by tearing of the fibers along their axes in liquid nitrogen. The iPP matrix around the VGCF nanofibers [Figure 5(c,d)] deviates from the typical spherulitic morphology and consists of row nucleated lamellae extending mainly in a perpendicular direction to the VGCF surface. This kind of morphology is very similar to that of the transcrystallites described by other authors.[26,30,31]

It is known that the VGCF surface can stimulate nucleation of the iPP lamellae that is the key factor of the transcrystallite morphology formation.[32] One can also expect that the iPP matrix in the transcrystalline layer should have noticeably different properties compared with those in the bulk matrix.

As known, the crystallization of iPP occurs by folding of the flexible polymer macromolecules. The main feature of the iPP crystalline structure is the formation of a unique cross-hatched morphology that was intensively investigated and described elsewhere.[33–35] An inset in the Figure 5(d) demonstrates such a morphology at higher magnification. A scheme showing different lamellae orientation in the cross-hatched morphology is represented in Figure 5(e). Such iPP crystallites are ascribed to α-modification which is common for iPP. The cross-hatched morphology consists of the following elements: (1) "mother" lamellae that start growing from the spherulite center or from

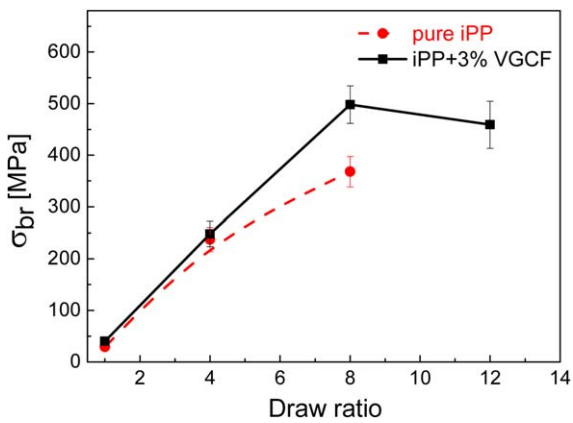

Figure 2. The influence of the draw ratio on the strength of the pure iPP and composite iPP + 3%VGCF fibers. [Color figure can be viewed in the online issue, which is available at wileyonlinelibrary.com.]

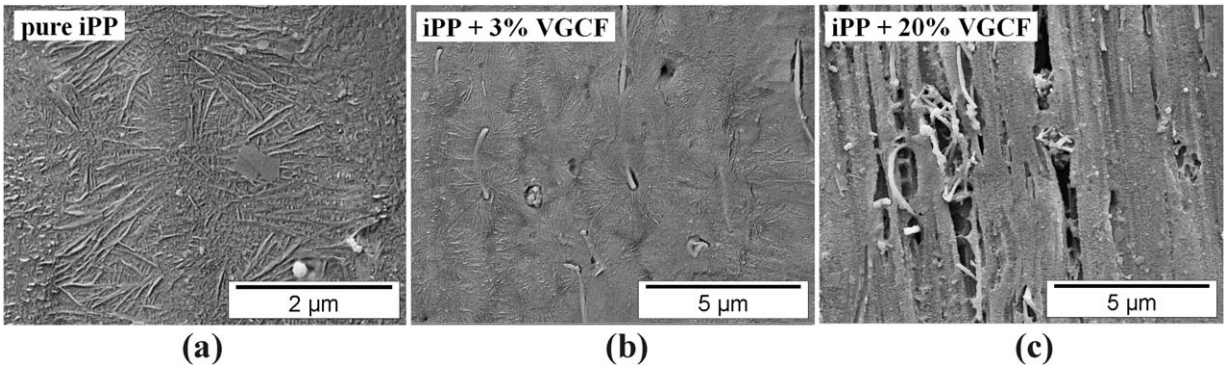

Figure 3. SEM micrographs of the surface structure of the undrawn pure iPP (a) and composite (b, c) fibers.

the surface of VGCF; (2) "daughter" lamellae that epitaxially grow on the surface of the "mother" lamellae. In the case of the composite iPP/VGCF melt-spun fibers, the "mother" lamellae are oriented perpendicularly to the VGCF surface and the "daughter" lamellae are, in turn, oriented along the VGCF. As mentioned above, in the investigated composite fibers the VGCF are rather well aligned in the extrusion direction, i.e. along the fiber axis. Therefore, one can conclude that the addition of VGCF leads to preferential nucleation in the surrounding iPP matrix and to oriented crystallite growth. This result indicates that the combined effect of VGCF aligned in the extrusion direction and of the preferential orientation of the iPP lamellae should generate a rather strong stiffening effect. The stiffening is evidently observed in the dependencies of σ_{br} on the VGCF content (Figure 1): the tensile strength of all composite fibers is higher than that of the pure iPP. However, it is also seen that the fibers with 20 wt % VGCF have the lowest σ_{br} among the other composite fibers. We believe that the reason of such strength reduction could be the fact that a large amount of VGCF hampers their good orientation during extrusion process that can also be seen in Figure 5(b).

In Figure 6 the internal structure of the oriented composite fiber with DR = 8 is presented. As known, during the orientation process the initial lamellae structure transforms into a fibrillar one.[36] This transformation can be accompanied by reorientation and breakage of the lamellae oriented perpendicularly to the drawing direction and, as the main transition proceeds, by unfolding of the polymer chains and their recrystallization followed by the micro- and macrofibril formation.[37,38] The microfibrils consisting of alternating crystalline and disordered regions are well seen in SEM images at higher magnification [Figure 6(b)]. No residuals of the original spherulitic and cross-hatched structures were found in the investigated fibers after hot drawing. It is worthy to note that the presence of the VGCF did not prevent the structural transformation in the iPP matrix, presumably because of the weak adhesion between VGCF and the iPP matrix. We assume that such a weak adhesion can also play a positive role when drawing a composite fiber. A stronger adhesion could certainly provide a much better stress transfer between the filler and the matrix during stretching in the undrawn state and, therefore, result in higher σ_{br} values. However, drawing of the composite fibers with stronger filler-matrix adhesion would be rather complicated.

As mentioned above, the composite fibers with 3 wt % VGCF were drawn up to DR = 12. We assume that in this case the VGCF could be regarded as defects similar to voids leading to easier slippage of the fully formed fibrils along each other. Such slippage does not improve the inner structure of the microfibrils themselves that results in the absence of the fiber strength enhancement at DR = 12 comparing to DR = 8 (Figure 2).

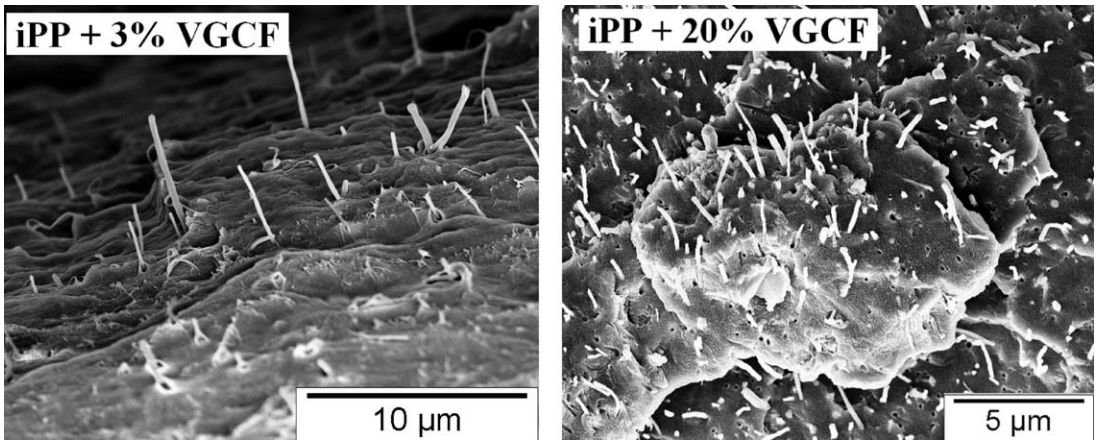

Figure 4. SEM micrographs of the cross-sections of the undrawn composite (3 wt % and 20 wt % VGCF) fibers.

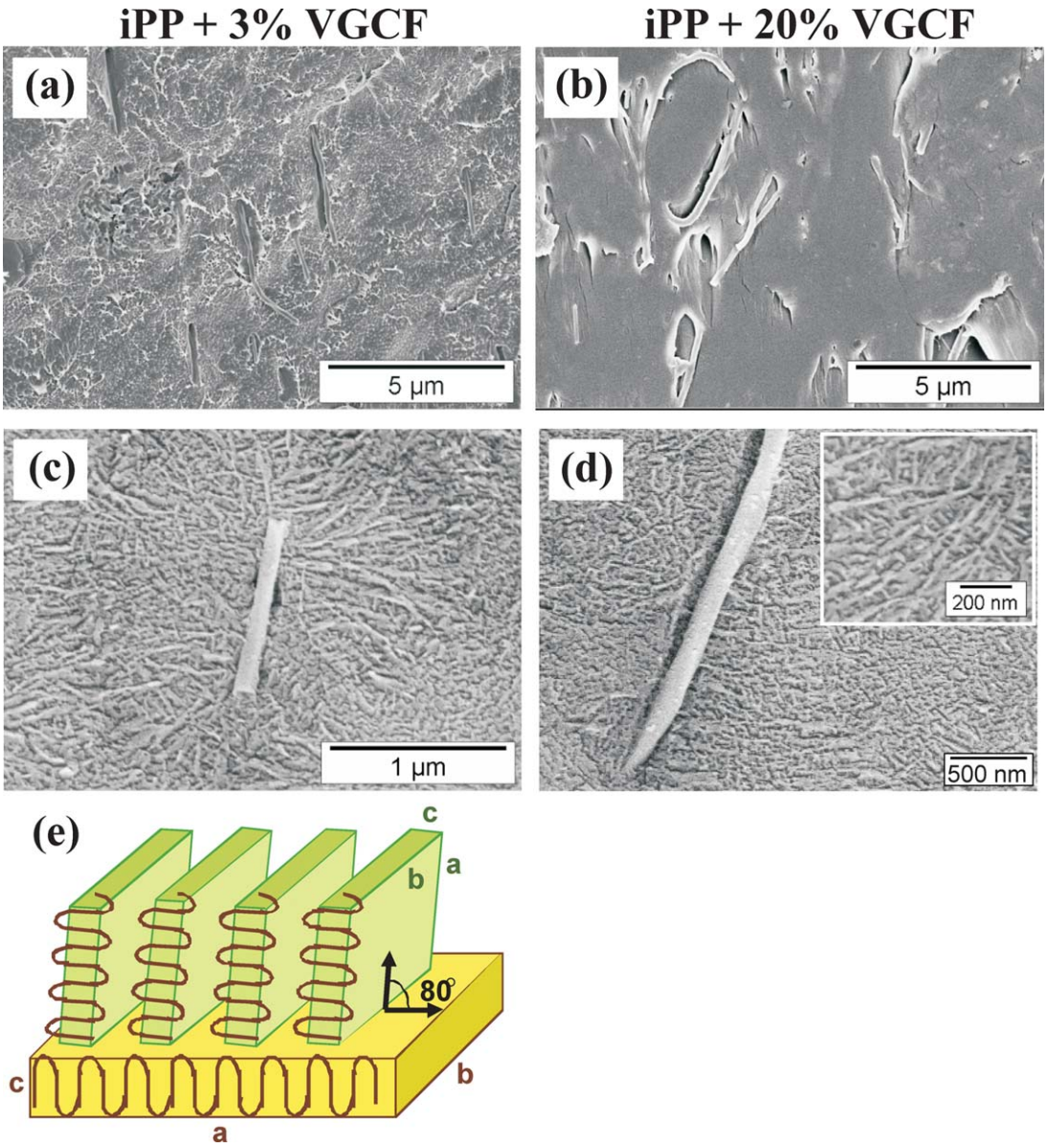

Figure 5. SEM micrographs of the internal structure of the undrawn composite fibers (3 wt % and 20 wt % VGCF) revealed after cryo-tearing of the fibers along their axes. The micrographs are presented at low (a, b) and higher (c, d) magnifications; a sketch of different lamellae orientation in the cross-hatched morphology (e). [Color figure can be viewed in the online issue, which is available at wileyonlinelibrary.com.]

In the pure iPP fiber the fibrillar slippage is inhibited, therefore, it could only be drawn up to DR = 8.

X-ray Diffraction Studies

As described above, the iPP matrix in all investigated fibers crystallized in the α-modification that was also confirmed by our WAXS data. The α-phase has a monoclinic unit cell with the following constants: $a = 6.65$ Å, $b = 20.78$ Å, $c = 6.5$ Å, $\beta = 99.6°$.[39] The *a-c* plane is the plane of the iPP chain folding.

Figure 7 demonstrates 2D WAXS patterns recorded from undrawn (DR = 1 – left part) and drawn (DR = 8 – right part) fibers. The typical Debye rings are revealed in the WAXS pattern of the pure iPP fiber in the undrawn state (DR = 1) (their pseudo-elliptical shape is due to the cylindrical shape of the detector). Addition of 1 wt % VGCF produces no strong effect on the textural properties. Starting from 3 wt % VGCF changes in the crystallite preferred orientation in undrawn fibers become detectable, i.e. the symmetric Debye rings partly transform in arcs. This implies an appearance of preferential orientation of iPP crystallites.

Addition of 20 wt % VGCF makes the texture more pronounced (especially it concerns the peak (002) of VGCF and the peaks (040), (111), and (13-1) of the iPP matrix). All these results confirm the idea that the presence of the VGCF nanofibers in the iPP matrix and their alignment along the main fiber axes lead to the appearance of the iPP crystallites, which are oriented in certain directions.

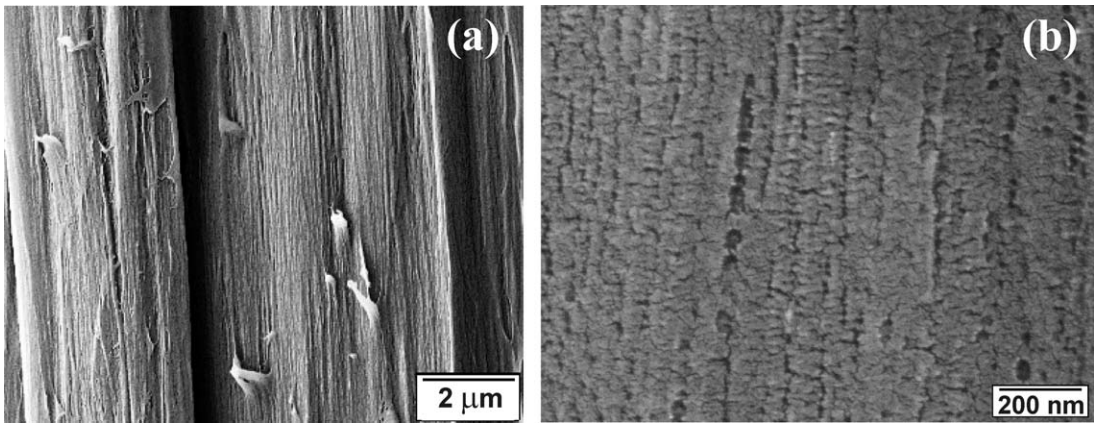

Figure 6. SEM micrographs of the inner structure of the drawn composite fiber (3 wt % VGCF) revealed after cryo-tearing along its axis. The micrographs are presented at low (a) and high (b) magnifications.

It should be noted that the 002 peaks of graphite (the only diffraction feature of VGCF visible in experimental WAXS patterns) display maxima in the equatorial direction confirming the preferential orientation of VGCF along the fiber axis. This agrees well with the results obtained by SEM and discussed above.

It is worthy to note that in the composite fibers containing 3 wt % VGCF and more the 110 Debye rings are split into two reflections: one of them is on the equator and the second is near the meridian. This phenomenon was intensively investigated and described in the literature.[40,41] It is proved that the equatorial 110 maxima correspond to the *c*-crystallites, which have their ***c***-axes oriented along the fiber direction—these are the "mother" transcrystallites starting to grow from the VGCF surface. The meridional 110 maxima are produced by the *a*-crystallites whose *a*-axes are oriented along the fiber direction—these are the "daughter" iPP crystallites which epitaxially grow on the "mother" transcrystallites. The *b*-axes of both kinds of crystallites are oriented in the same direction—perpendicularly to the VGCF axes. This is in line with the relatively weak change in the 040 reflections with increasing VGCF content.

Looking at the right parts of the WAXS patterns in Figure 7 one can conclude that the iPP matrix was totally recrystallized during hot drawing and newly formed crystallites are rather well oriented in the fiber direction (as it was previously shown in SEM micrographs in Figure 6). The 1D WAXS diffraction patterns taken in the equatorial direction allow estimation of the sizes of the iPP crystallites (coherently diffracting domains). To avoid overloading this paper with figures, we do not present here the experimental 1D WAXS patterns and only report the values of the transverse crystallite sizes D_{110} (along the direction normal to the 110 planes), estimated with the use of the Scherrer formula. These sizes for both undrawn and drawn fibers depend on the VGCF content [Figure 8(a,b)] in a nonmonotonic way: in both cases (DR = 1 and 8) the maxima at 3 wt % VGCF are clearly observed. It should also be noted that for the undrawn fibers, the D_{110} versus %VGCF curve is very similar to that of σ_{br} versus %VGCF for the drawn fibers in Figure 1(b). The similar behavior of the functions D_{110} (%VGCF) for DR = 1 and σ_{br} (%VGCF) for DR = 8 indicates that the mechanical properties (i.e. tensile strength) of the final drawn

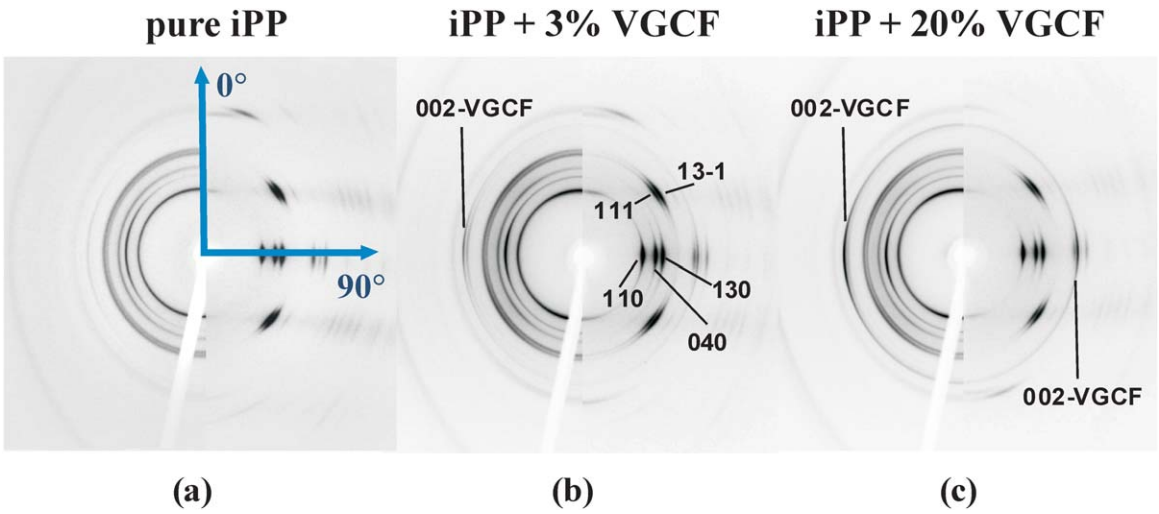

Figure 7. Two-dimensional WAXS diffraction pattern of the pure iPP (a) and composite (b, c) fibers. The fibers were studied in undrawn (left side) and drawn (right side) states. [Color figure can be viewed in the online issue, which is available at wileyonlinelibrary.com.]

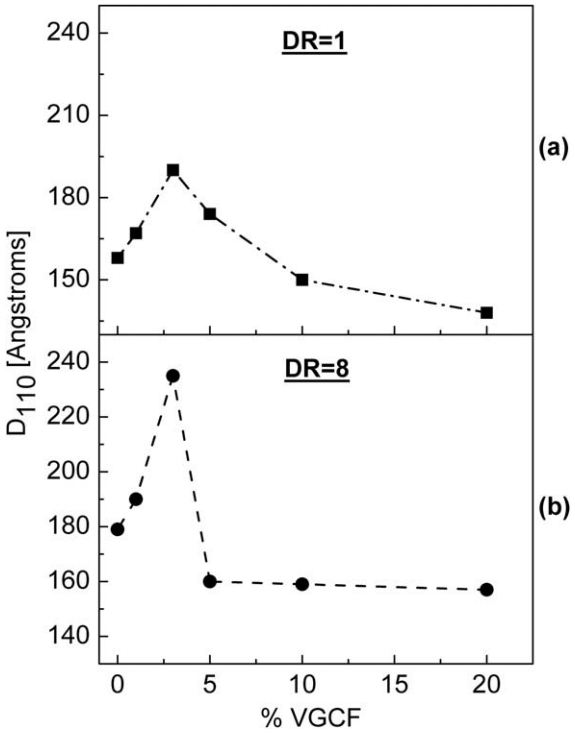

Figure 8. The dependence of the crystalline size D_{110} on the VGCF content of undrawn (a) and drawn (b) fibers.

fibers are strongly affected in this region by the orientation and sizes of the crystallites in the original undrawn iPP matrix.

At DR = 8 the value of D_{110} also displays a maximum at 3 wt % VGCF. One can conclude that the largest crystalline regions inside iPP microfibrils can be obtained during drawing of the composite iPP + 3%VGCF fibers. Therefore, the presence of large crystallites surely must lead to significant changes in the mechanical properties. In the fibers with the highest content of the filler (iPP + 20%VGCF) the crystallite sizes in both the undrawn (DR = 1) and drawn (DR = 8) states have the lowest values compared with all other fibers. It can be explained so that the high content of the VGCF in the undrawn fiber reduces the iPP lamellae length due to a decrease in the average distance between VGCF nanofibers and, therefore, the crystallization of

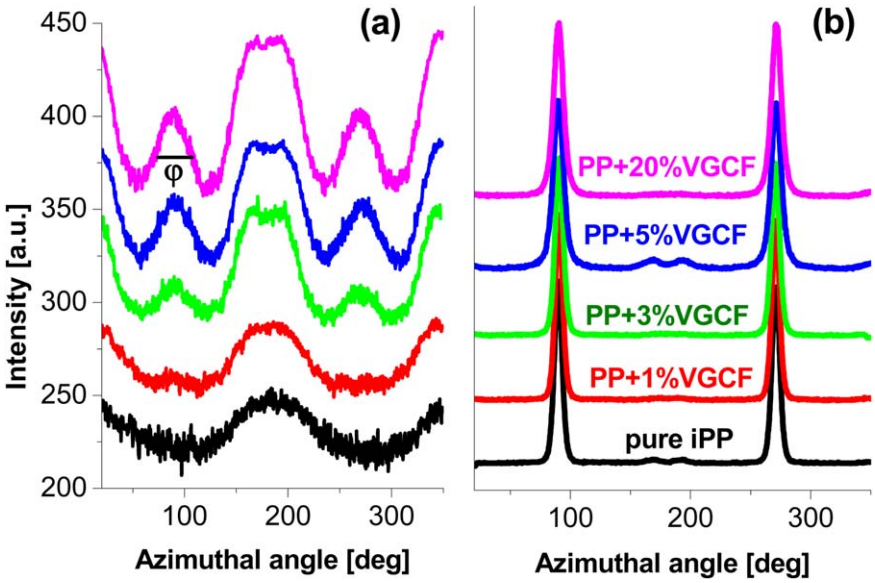

Figure 9. Azimuthal profiles of the 110 WAXS reflections of the pure iPP and composite iPP + VGCF fibers: (a) DR = 1; (b) DR = 8. The azimuthal angle scale corresponds to the marks seen in Figure 7(a) (meridional direction: 0°, 180°; equatorial direction: 90°, 270°). The intensity was measured in two-dimensional WAXS patterns shown in Figure 7. The color coding is the same in both (a) and (b). [Color figure can be viewed in the online issue, which is available at wileyonlinelibrary.com.]

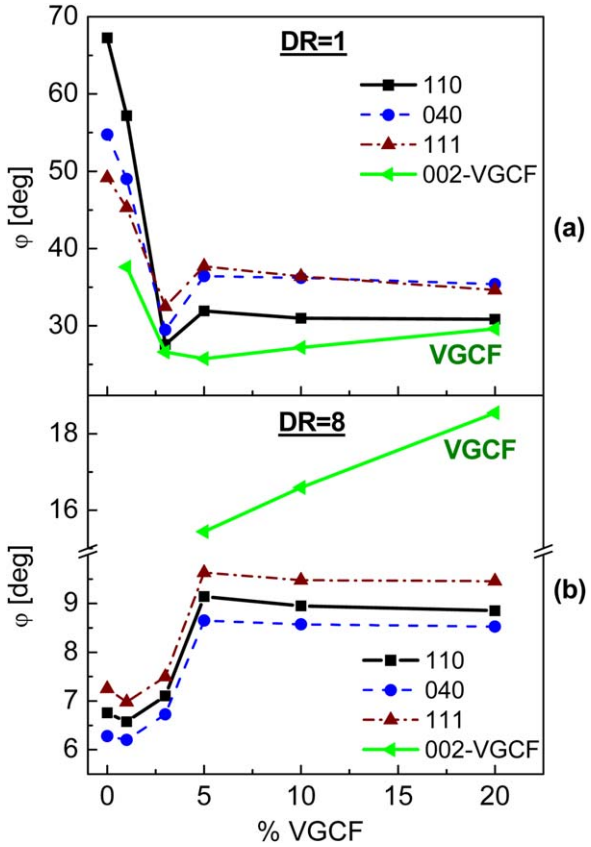

Figure 10. The dependence of the misorientation angle φ on the VGCF content of undrawn (a) and drawn (b) composite fibers. [Color figure can be viewed in the online issue, which is available at wileyonlinelibrary.com.]

the iPP matrix occurs in confined conditions. Another important factor is the orientation of the VGCF, which is far from being perfect [see Figure 5(b)]. This means that many lamellae are located in the positions unsuitable for unfolding and recrystallization during further drawing process.

Coming back to the original two-dimensional WAXS results (Figure 7), it would be very desirable to quantitatively estimate the degree of the overall orientation of α-crystallites in all investigated fibers. This is possible to do using azimuthal scans of the diffraction rings or arcs—in this case the arcs appear as peaks. Figure 9 demonstrates the WAXS azimuthal profiles (along the Debye rings) recorded from the undrawn DR = 1 fibers [Figure 9(a)] and from the drawn DR = 8 ones [Figure 9(b)]. The strong dependence of the azimuthal distribution of the scattered intensity of the 110 iPP reflection on the VGCF content is clearly seen. At the fraction of VGCF 3 wt % or more the ordered splitting of the 110 reflection is observed (as it was discussed earlier). It should be noted that the broad peaks at 180° correspond to the meridional 110 reflections, which, in turn, answer the "daughter" iPP lamellae oriented with their basal planes (110) along the fiber direction. Certain amount of the oriented "daughter" lamellae is also found in the neat iPP fibers indicating the presence of small orientation of iPP crystallites after the fiber extrusion. As for the oriented fibers, their azimuthal 110 profiles are very similar: they display two equatorial peaks with the full widths at half-maximum (FWHM) dependent on the content of VGCF.

The peaks of azimuthal intensity distribution (texture maxima) have been fitted with pseudo-Voigt functions and their FWHMs have been measured to quantify the sharpness of the corresponding texture. This value can be interpreted as a mean angle φ of the crystallite misorientation (deviation of the corresponding crystallographic direction from the direction along or normal to the fiber axis).[42] The broader the azimuthal peak (i.e. the higher value of misorientation angle φ), the smaller the orientation degree of the crystallites with respect to the fiber axis.

The resulting dependencies of the misorientation angle φ on the VGCF content for the undrawn (DR = 1) and drawn (DR = 8) fibers are presented in Figure 10(a,b). In both figures very strong effects of the filler content and of the drawing on the orientation degree of the crystallites can be observed.

From Figure 10 it can be concluded that the orientation of the VGCF themselves is also dependent on their amount. In fact, as

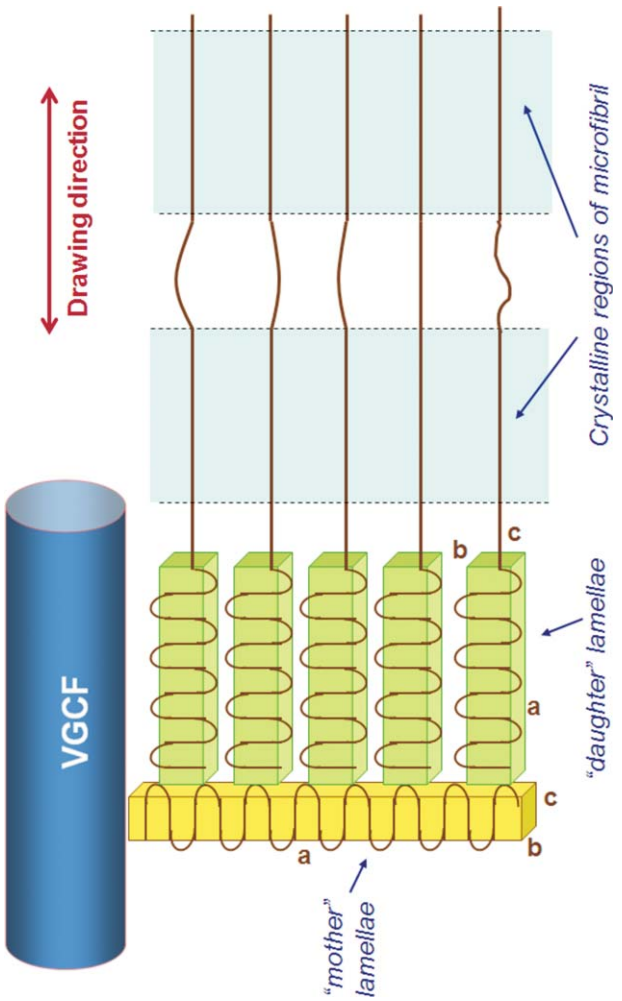

Figure 11. Scheme of the drawing process of the composite iPP + VGCF fiber. [Color figure can be viewed in the online issue, which is available at wileyonlinelibrary.com.]

it was observed by SEM [Figure 3(c)], at high concentration of the filler (i.e. 20 wt % VGCF) the orientation of the nanofibers becomes less ordered during extrusion. The most significant impact of the VGCF on the crystallite orientation is observed at 3 wt % VGCF. A further increase in VGCF amount ($\geq$5 wt % VGCF) leads to increased misorientation of the crystallites as a result of the lowering orientation degree of the VGCF inside the main fiber.

A similar situation is found in the drawn pure and composite fibers in Figure 10(b). It is necessary to note that the drawing process produces the fibers with much lower values of misorientation angle φ, i.e. with much higher orientation degree of the iPP crystallites and VGCF. However, in contrast to the undrawn case, the misorientation in the fibers with DR = 8 increases drastically when the VGCF content exceeds 5 wt %. As discussed earlier, a large number of VGCF and their imperfect orientation in the original undrawn state hampers further drawing and orientation of the recrystallized iPP matrix.

Summing up all the experimental data described above, we propose the following scheme of the composite sample structure (Figure 11). It should be kept in mind, however, that one-dimensional-WAXS diffraction profiles recorded in the equatorial plane were used to estimate the crystallite sizes in the direction normal to the (110) crystallographic planes. Therefore, Figure 9 shows the distribution of the crystallite sizes mostly for the "mother" lamellae which grew perpendicularly to the VGCF. However, since such lamellae are located in a very unsuitable position for the further hot drawing and polymer chain unfolding, they cannot be easily unfolded and recrystallized. From this point of view, the largest crystallite sizes D_{110} observed for the composite fibers with 3 wt % VGCF should not play any positive role in the specimen strengthening. During drawing process such long lamellae will break in smaller pieces which could be able to rotate and to re-orient themselves in a position suitable for chain unfolding (i.e. along the fiber axis) as described in Ref. 37. The breakage and rotation of the lamellae is associated with microvoid formation. In this case the strength of the composite fibers should drop.

On the other hand, in Figure 1 an opposite effect is observed at 3 wt % VGCF. The scheme presented here can easily explain this experimental fact as follows: the longer the "mother" transcrystallites have formed, the larger number of the "daughter" lamellae can epitaxially grow on their surface. These "daughter" lamellae have their *a*–*c* planes (i.e. the planes of their macromolecule folding) parallel to the drawing direction. Therefore, the polymer chains in these lamellae can easily and simultaneously straighten with following recrystallization and formation of well-oriented microfibrils consisting of extended chains with low amount of defects. In this case we assume that the amorphous parts of the microfibrils, which are responsible for the tensile strength of the investigated fibers, should also be less defective. The influence of the microvoids formed from the "mother" lamellae will be overcompensated by the orientation of the microfibrils. If the resulting oriented fiber has such a well-arranged microfibrillar structure, then its strength will be considerably increased. Therefore, a very important conclusion can be drawn: the improvement in the mechanical properties (i.e. the tensile strength) of the composite fibers is attributed not to the VGCF reinforcing effect, but mainly to the specially oriented crystalline structure (both in the undrawn and drawn states) induced by the presence of the VGCF filler.

CONCLUSIONS

From the data presented above the following conclusions can be drawn:

1. The VGCF filler evidently affects the crystalline structure of the iPP + VGCF composite fibers leading to considerable changes in their mechanical properties.
2. The lamellae nucleation process determines the degree of the crystallite orientation in both undrawn and drawn states.
3. The overall orientation degree of the α-crystallites is strongly effected by the VGCF content and drawing.
4. All the mechanical improvements are dependent on the VGCF content in the composite fibers and ascribed mainly to the changes in the crystalline microstructure of the iPP matrix rather than to a reinforcement role of VGCF, which is negligible due to very low adhesion between the filler and the iPP matrix.

It is planned to prolong the work and investigate in more detail an effect of the orientational drawing on the fine structure of the composite fibers.

This study has been supported by the Russian Ministry of Education and Science within State Contract No. 14.Z50.31.0002 (megagrant of the Government of the Russian Federation according to the Resolution No. 220 of April 9, 2010). The X-Ray diffraction experiments have been performed at the Research Center for X-Ray Diffraction Studies, Saint Petersburg State University. Dr. Alexander N. Bugrov is kindly acknowledged for the help with sample preparation for SEM experiments. The authors are very grateful Prof. Ekaterina S. Tsobkallo and Prof. Irina P. Dobrovol'skaya for useful discussion of the results obtained.

REFERENCES

1. Lozano, K.; Bonilla-Rios, J.; Barrera, E. V. *J. Appl. Polym. Sci.* **2001**, *80*, 1162.
2. Kuriger, R. J.; Alam, M. K.; Anderson, D. P.; Jacobsen, R. L. *Compos. A* **2002**, *33*, 53.
3. Hammel, E.; Tang, X.; Trampert, M.; Schmitt, T.; Mauthner, K.; Eder, A.; Potschke, P. *Carbon* **2004**, *42*, 1153.
4. Hine, P.; Broome, V.; Ward, I. *Polymer* **2005**, *46*, 10936.
5. Yang, S.; Lozano, K.; Lomeli, A.; Foltz, H. D.; Jones, R. *Compos. A* **2005**, *36*, 691.
6. Kumar, S.; Doshi, H.; Srinivasarao, M.; Park, J. O.; Schiraldi, D. A. *Polymer* **2002**, *43*, 1701.
7. Kuriger, R. J.; Alam, M. K.; Anderson, D. P. *J. Mater. Res.* **2001**, *16*, 226.
8. Chirila, V.; Marginean, G.; Iclanzan, T.; Merino, C.; Brandl, W. *J. Therm. Comp. Mater.* **2007**, *20*, 277.

9. Zeng, J.; Saltysiak, B.; Johnson, W. S.; Schiraldi, D. A.; Kumar, S. *Compos. B* **2003**, *35*, 173.
10. Lopez Manchado, M. A.; Valentini, L.; Biagiotti, J.; Kenny, J. M. *Carbon* **2005**, *43*, 1499.
11. Kearns, J. C.; Shambaugh, R. L. *J. Appl. Polym. Sci.* **2002**, *86*, 2079.
12. Tibbetts, G. G.; McHugh, J. J. *J. Mater. Res.* **1999**, *14*, 2871.
13. Lozano, K.; Barrera, E. V. *J. Appl. Polym. Sci.* **2001**, *79*, 125.
14. Katerelos, D. T. G.; Joffe, R.; Labou, D.; Wallstrom, L. *Mech. Comp. Mater.* **2009**, *45*, 423.
15. Sui, G.; Zhong, W. H.; Fuqua, M. A.; Ulven, C. A. *J. Appl. Polym. Sci.* **2008**, *107*, 2837.
16. Lee, S.; Hahn, J. R.; Ku, B. C.; Kim, J. K. *Korean Chem. Soc.* **2011**, *32*, 2369.
17. Sandler, J.; Broza, G.; Nolte, M.; Schulte, K.; Lam, Y. -M.; Shaffer, M. S. P. *J. Macromol. Sci. Part B: Phys.* **2003**, *42*, 479.
18. Bhattacharyya, A. R.; Sreekumar, T. V.; Liu, T.; Kumar, S.; Ericson, L. M.; Hauge, R. H.; Smalley, R. E. *Polymer* **2003**, *44*, 2373.
19. Dondero, W. E.; Gorga, R. E. *J. Polym. Sci. Part B: Polym. Phys.* **2006**, *44*, 864.
20. Valentini, L.; Biagiotti, J.; Kenny, J. M.; Santucci, S. *J. Appl. Polym. Sci.* **2003**, *87*, 708.
21. Pinchuk, L. S.; Goldade, V. A.; Vinidiktova, N. S.; Choi, U. S.; Hong, S. Ch. *Mech. Comp. Mater.* **2005**, *41*, 171.
22. Valentini, L.; Biagiotti, J.; Kenny, J. M.; Santucci, S. *Compos. Sci. Technol.* **2003**, *63*, 1149.
23. Chipara, M. D.; Lozano, K.; Hernandez, A.; Chipara, M. T. G. A. *Polym. Degrad. Stab.* **2008**, *93*, 871.
24. Zhao, Q.; Wagner, H. D. *Philos. Trans. R. Soc. Lond. A* **2004**, *362*, 2407.
25. Kolb, R.; Seifert, S.; Stribeck, N.; Zachmann, H. G. *Polymer* **2000**, *41*, 1497.
26. Larin, B.; Lyashenko, T.; Harel, H.; Marom, G. *Compos. Sci. Technol.* **2011**, *71*, 177.
27. Showa Denko Carbon Inc., Vapor Grown Carbon Fiber. Available at: http://sdkc.com/documents/VGCF-H.pdf. Accessed December 25, 2014.
28. Bassett, D. C.; Olley, R. H. *Polymer* **1984**, *25*, 935.
29. Balta-Calleja, F. J.; Vonk, C. G.; X-ray Scattering of Synthetic Polymers; Elsevier Science Publishers: Amsterdam, **1989**, p 241.
30. Ning, N.; Fu, S.; Zhang, W.; Chen, F.; Wang, K.; Deng, H.; Zhang, Q.; Fu, Q. *Prog. Polym. Sci.* **2012**, *37*, 1425.
31. Campbell, D.; Qayyum, M. M. *J. Polym. Sci.: Polym. Phys. Ed.* **1980**, *18*, 83.
32. Li, H.; Yan, S. *Macromolecules* **2011**, *44*, 417.
33. Norton, D. R.; Keller, A. *Polymer* **1985**, *26*, 704.
34. Binsbergen, F. L.; De Lange, B. G. M. *Polymer* **1968**, *9*, 23.
35. Olley, R. H.; Bassett, D. C. *Polymer* **1989**, *30*, 399.
36. Marikhin, V. A.; Myasnikova, L. P. In Oriented Polymer Materials; Fakirov, S., Ed.; Hüthig & Wepf: Heidelberg, **1996**; Chapter 2, p 38.
37. Henning, S.; Michler, G. H.; Ania, F.; Balta-Calleja, F. J. *Colloid Polym. Sci.* **2005**, *283*, 486.
38. Marikhin, V. A.; Myasnikova, L. P. *Progr. Colloid Polym. Sci.* **1993**, *92*, 39.
39. Lotz, B.; Wittmann, J. C. *J. Polym. Sci.* **1986**, *24*, 1541.
40. Clark, E. S.; Spruiell, J. E. *Polym. Eng. Sci.* **1976**, *16*, 176.
41. Lovinger, A. J. *J. Polym. Sci.: Polym. Phys. Ed.* **1983**, *21*, 97.
42. Frommert, M.; Zobrist, C.; Raabe, D.; Zaefferer, S.; Lahn, L.; Böttcher, A. In Materials Processing and Texture: Ceramic Transactions; Rollett, A. D., Ed.; John Wiley and Sons: New Jersey, **2008**; p. 143.